2015

Combined analysis of soil moisture measurements from roving and fixed cosmic ray neutron probes for multiscale real-time monitoring

Trenton E. Franz
University of Nebraska-Lincoln, trenton.franz@unl.edu

Tiejun Wang
University of Nebraska - Lincoln

William Avery
University of Nebraska - Lincoln

Catherine E. Finkenbiner
University of Nebraska-Lincoln, c.finkenbiner@gmail.com

Luca Brocca
Istituto di Ricerca per la Protezione Idrogeologica

Used by permission.

Combined analysis of soil moisture measurements from roving and fixed cosmic ray neutron probes for multiscale real-time monitoring

Trenton E. Franz[1], Tiejun Wang[1], William Avery[1], Catherine Finkenbiner[1], and Luca Brocca[2]

[1]School of Natural Resources, University of Nebraska–Lincoln, Lincoln, Nebraska, USA, [2]Istituto di Ricerca per la Protezione Idrogeologica, Perugia, Italy

Abstract Soil moisture partly controls land-atmosphere mass and energy exchanges and ecohydrological processes in natural and agricultural systems. Thus, many models and remote sensing products continue to improve their spatiotemporal resolution of soil moisture, with some land surface models reaching 1 km resolution. However, the reliability and accuracy of both modeled and remotely sensed soil moisture require comparison with ground measurements at the appropriate spatiotemporal scales. One promising technique is the cosmic ray neutron probe. Here we further assess the suitability of this technique for real-time monitoring across a large area by combining data from three fixed probes and roving surveys over a 12 km × 12 km area in eastern Nebraska. Regression analyses indicated linear relationships between the fixed probe averages and roving estimates of soil moisture for each grid cell, allowing us to derive an 8 h product at spatial resolutions of 1, 3, and 12 km, with root-mean-square error of 3%, 1.8%, and 0.9%.

1. Introduction

Knowledge of soil moisture fields is critical for understanding the exchange of mass between the land surface and atmosphere and thus the link between soil moisture state and planetary boundary layer regime, clouds, and precipitation [*Santanello et al.*, 2011]. With the continued refinement of land surface models (LSM) to grid sizes less than 1 km [*Wood et al.*, 2011], there remains a significant scale gap [*Ochsner et al.*, 2013] between available point sensor networks (i.e., Soil Climate Analysis Network, High Plains Regional Climate Center, and Oklahoma Mesonet [*Ford and Quiring*, 2014]) and remote sensing products from satellites (i.e., SMOS and SMAP [*Crow et al.*, 2012]). Such information is essential for model calibration and validation as well as specifying the initial conditions for data assimilation and weather forecasting.

Accurate estimates of soil moisture fields at 1 km resolution have until recently been difficult to obtain [*Chrisman and Zreda*, 2013]. The cosmic ray neutron probe (CRNP) offers a new spatial scale to observe how soil moisture fields are structured given its support area of ~0.28 km^2 [*Desilets and Zreda*, 2013], effective penetration depth of ~10 to 40 cm [*Franz et al.*, 2012], and roving capabilities [*Dong et al.*, 2014]. Given the fractal nature of soil moisture fields [*Rodriguez-Iturbe et al.*, 1995], combining this new observation scale with existing point and remote sensing products has the potential to provide further insight into deriving any scale invariant relationships that may exist, as well as key statistical moments of soil moisture fields at LSM grid resolutions. Moreover, an a priori estimate of the temporal and spatial soil moisture covariance matrices at different averaging scales will be invaluable for statistical downscaling procedures [*Wood et al.*, 2004] of remotely sensed soil moisture products.

Using basic statistical approaches, we combine data from three fixed CRNP and 22 rover surveys over a 12 km × 12 km area between May and September 2014 in eastern Nebraska, where the predominant land use is agriculture. The goal of this work was to lay the foundation for the design of cost-effective real-time soil moisture monitoring networks that fill in the gap between point sensors and remote sensing products. Using the observations, we derive statistical relationships for the entire study area with grid resolutions of 1, 3, and 12 km, allowing us to construct a real-time proximal sensing monitoring network. In this work, we will describe the soil moisture network design within the study area, processing of fixed and roving cosmic ray neutron data in agricultural settings, the spatiotemporal statistics of the observed soil moisture fields, and the spatial regression procedure using data merging.
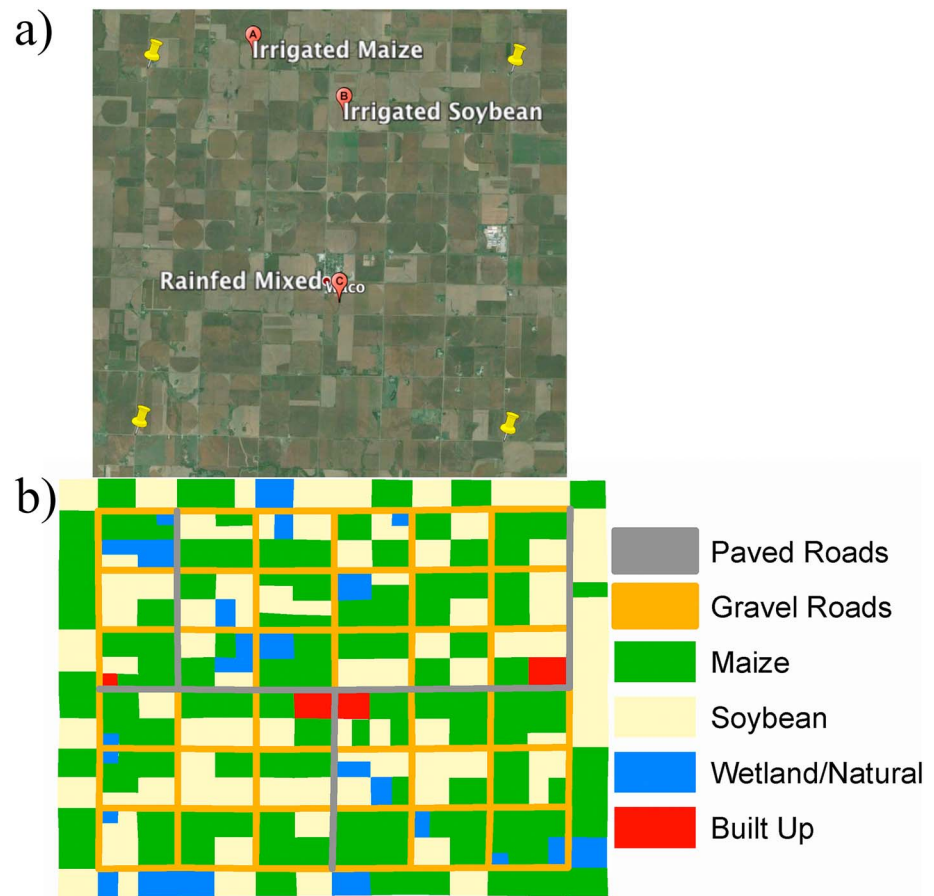
Figure 1. (a) Location of the 12 km × 12 km study area (defined by yellow pins) in eastern Nebraska and the three fixed CRNP in irrigated maize, irrigated soybean, and rainfed mixed. (b) The 2014 land cover map classifying the study area into four categories and illustrating the 1.6 km network of gravel and paved roadways.

2. Study Area

A soil moisture-monitoring network was set up over a 12 km × 12 km area around Waco, NE, USA (center of the study area 40.8976°N, 97.4604°W; Figure 1a). Because of the intense agricultural production, the study area contains a square lattice of paved and gravel roads at 1.6 km spacing (Figure 1b), making the location an ideal setting for roving CRNP surveys from a vehicle. The land use in the study area is a mixture of built up urban areas (1.26%), natural wetlands (8.03%), and irrigated maize (51.82%), and irrigated soybean (38.89%), partitioned by quarter section areas or smaller (Figure 1b). The dominant form of irrigation is with center-pivot sprinklers. Given the available growing season rainfall in the study area, seasonal irrigation is often supplemental with the highest use periods beginning in early July and continuing through August. The 2014 growing season (May to September) was a relatively wet year (772 mm between April 20 and September 20, data available from the High Plains Regional Climate Center at York, NE) with widespread irrigation only occurring between late July and mid-August with a total applied irrigation depth of 94 mm for the irrigated maize site and 82.6 mm for the irrigated soybean site occurring over five and four center-pivot passes, respectively (Chase Johnson, personal communication, 2014).

3. Sampling and Network Design

Three fixed CRNP (model #CRS 2000/B from Hydroinnova LLC, Albuequerque, NM USA) were set up in late April 2014 at an irrigated maize field (40.9482°N, 97.4875°W), an irrigated soybean field (40.9338°N, 97.4587°W), and a rainfed mixed maize and soybean field (40.8899°N, 97.4586°W) within the study area (Figure 1a). At each site, hourly values of moderated neutron counts, air pressure, air temperature, and
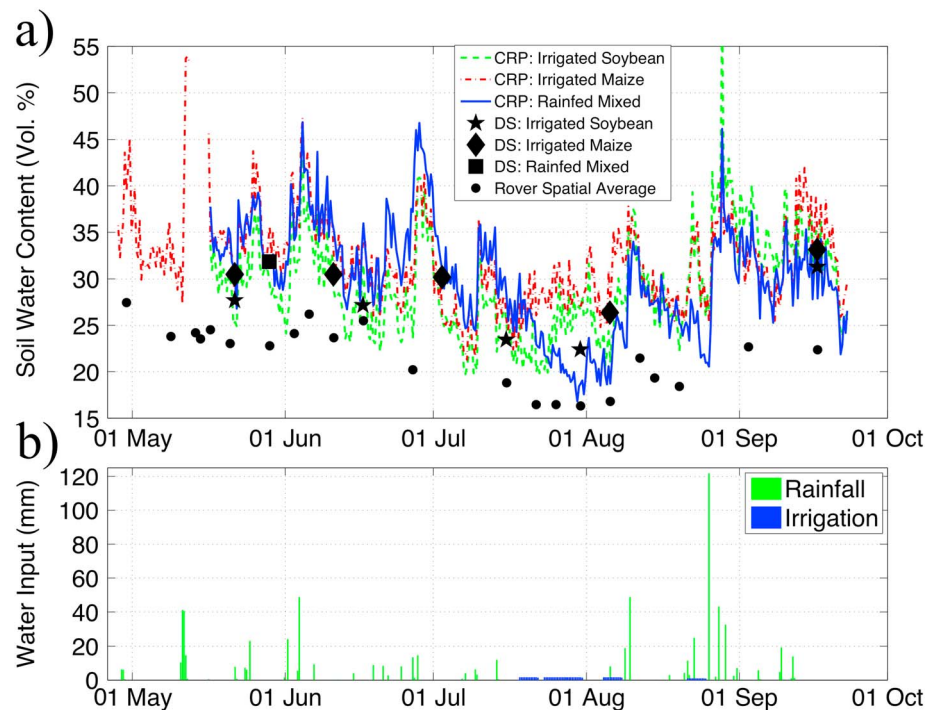
Figure 2. (a) Comparison of soil water content from the three fixed CRNP (green, red, and blue lines) and average from the 22 CRNP rover surveys (black dots) between May and September 2014. Gravimetric estimates from calibration data sets are also shown (black diamonds, black stars, and black square). All data sets are provided in Tables S1, S2, S3, and S6 in the supporting information. (b) Time series of rainfall and irrigation water inputs.

relative humidity were recorded for processing [*Zreda et al.*, 2012]. Over the course of the growing season, 11 calibration data sets (5 at each of the two irrigated sites and 1 at the rainfed site) were collected for variables of area average gravimetric water content, soil bulk density, soil lattice water, soil organic carbon, wet aboveground biomass, and dry aboveground biomass following established protocols [*Zreda et al.*, 2012], see Figure 2 and Table S1 in the supporting information for full data sets. Calibration sampling duration took between 2 and 4 h to complete on each sampling day.

Between 29 April and 16 September 2014, 22 mobile CRNP surveys were collected across the study site. The cosmic ray rover is composed of eight specially designed extra long (~1.8 m as compared to ~0.9 m) CRS 2000/B tube capsules and has counting rates are approximately 11 times greater than the original CRS 2000/B model, allowing for 1 min level measurements with sufficiently low uncertainty (~350 c/min with an uncertainty of ~ 5%). The eight capsules are mounted on a custom vibration-minimizing frame, which is bolted to the bed of a vehicle. Air temperature, air pressure, relative humidity, and location (with an accuracy of <10 m) were also recorded at 1 min intervals. During a rover survey, the vehicle was driven at a maximum speed of 0.8 km/min (i.e., in order to have a reasonable density of grid points for spatial interpolation to ~1 km), first in a north-south boustrophedonic pattern, then followed by an east-west survey, see Figures 3a and 3b for example survey points and spatially interpolated neutron count fields. Given the use of heavy equipment and routine maintenance of gravel roads, road closures often occurred requiring the vehicle to double-back and/or periodically skip certain sections. In general, rover surveys took between 4 and 6 h to complete resulting in between 240 and 360 neutron count observation points. Start times of the surveys varied between 9 A.M. and noon local time. Because of the required time to collect a rover survey (4 h) and calibration data set (2–4 h), all statistically derived data products have a time resolution of 8 h. Future work may be able to further reduce the temporal resolution of the data products.

4. Cosmic Ray Neutron Data Processing for Soil Moisture Estimation

Fixed and roving moderated neutron counts were first corrected for location (i.e., neutron scaling factor), incoming high-energy particles, atmospheric pressure, and absolute humidity following established
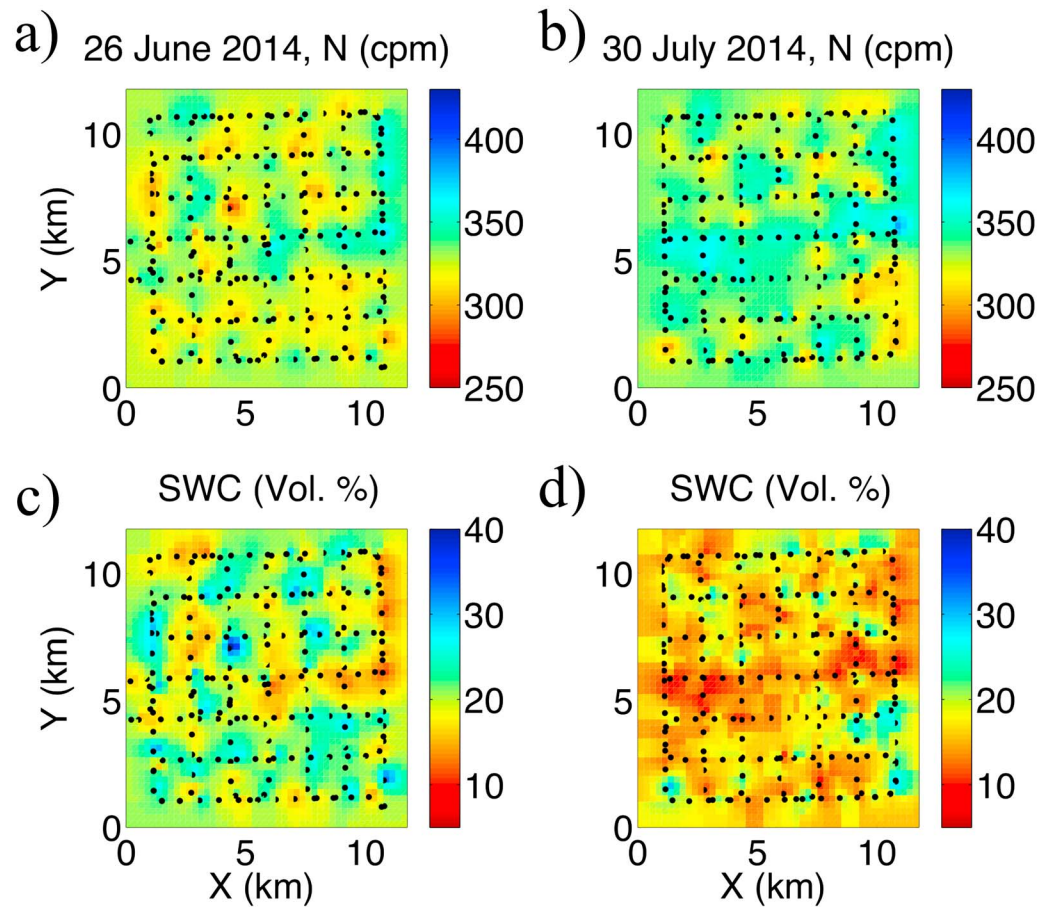
Figure 3. (a and b) Neutron count field and corresponding (c and d) soil water content for a rainfed (Figures 3a and 3c) and irrigated period (Figures 3b and 3d). The black dots correspond to measurement locations. Rover data sets are provided in Table S6 in the supporting information.

protocols [*Zreda et al.*, 2012]. The corrected neutron counts were then converted to volumetric pore water content using the calibration function originally proposed by [*Desilets et al.*, 2010] and further modified by [*Bogena et al.*, 2013]. The calibration function is given by

$$\left(\theta_p + \theta_{\text{LW}} + \theta_{\text{SOC}_{\text{eq}}}\right) = \frac{0.0808}{\frac{N}{N_0[f(\text{BWE})]} - 0.372} - 0.115 \tag{1}$$

where θ_p is pore water content (g/g), θ_{LW} is lattice water content (g/g), $\theta_{\text{SOC}_{\text{eq}}}$ is soil organic carbon water content equivalent (g/g), N is the corrected neutron counts per time interval (cph or cpm), N_0 is a specific calibrated parameter that represents the count rate over dry silica soils (cph or cpm) and is a function of BWE, and BWE is the biomass water equivalent (mm). We note that soil water content (SWC) = volumetric water content and that SWC $= \theta_p * \frac{\rho_b}{\rho_w}$ (cm³/cm³), where ρ_b is the dry soil bulk density (g/cm³), ρ_w is the density of water (=1 g/cm³), and we report here the SWC on a percent volume basis for convenience of units. Soil organic carbon water content equivalent is estimated from on-site soil chemistry sampling as

$$\theta_{\text{SOC}_{\text{eq}}} = (\text{TC} - \text{TIC})*1.724*f_{\text{WE}} \tag{2}$$

where TC is the soil total carbon (g/g), TIC is the inorganic carbon determined by measuring CO_2 after the sample is acidified (g/g), 1.724 is a constant to convert total organic carbon into total organic matter, and $f_{\text{WE}} = 0.494$ is the stoichiometric ratio of H_2O to organic carbon (assuming organic carbon is cellulose $C_6H_{10}O_5$) [*Nelson and Sommers*, 1996].

From the calibration data sets, we found that a linear function can be used to describe the dependence of changing biomass on N_0 for both maize and soybean. In addition, we choose here to provide a scaled

relationship to the rover observations in order to remove any sensor to sensor bias that may exist [*McJannet et al.*, 2014]. We correct for variations between instruments and for changes in BWE by scaling the fixed probe observations against the rover:

$$N_{0,F}(\mathrm{BWE}) = N_{0,F}(0)\left(\frac{m_R}{N_{0,R}(0)}\mathrm{BWE} + 1\right) \qquad (3)$$

where $N_{0,F}(0)$ is the fixed probe estimate of N_0 with no standing biomass, $N_{0,R}(0)$ is the rover estimate of N_0 with no standing biomass, and m_R is the slope of the relationship between N_0 and BWE from the rover surveys and calibration data sets. We note that for the rover survey points, $N_{0,F}(0) = N_{0,R}(0)$, further simplifying equation (3). The BWE was found from the calibration sampling as

$$\mathrm{BWE} = \mathrm{SWB} - \mathrm{SDB} + \mathrm{SDB}*f_{\mathrm{WE}} \qquad (4)$$

where SWB is the standing wet biomass per unit area (kg/m^2 ~ mm of water/m^2) and SDB is the standing dry biomass per unit area (kg/m^2 ~ mm of water/m^2) found by ovendrying samples at 70°C for 5 days. From the available calibration data sets, we found that the rover had a statistically significant linear relationship yielding the coefficients of $N_{0,R}(0) = 518.34$ cpm and $m_R = -4.9506$ with an $R^2 = 0.515$ and P value = 0.03, see Table S2 in the supporting information for full rover and fixed calibration data sets and neutron count observations. From the available calibration data sets, we found that the irrigated maize field had an $N_{0,F}(0)$ = 2771 cph, the irrigated soybean field had an $N_{0,F}(0)$ = 2796 cph, and the rainfed mixed field had an $N_{0,F}(0)$ = 2642 cph, where the differences in $N_{0,F}(0)$ values likely represent sensor to sensor differences in counting efficiency. This efficiency difference is accounted for in equation (3) by the term $\frac{N_{0,F}(0)}{N_{0,R}(0)}$. We further note that the other sources of error from the calibration procedure and neutron counting uncertainty will be lumped into this relationship through the estimation of N_0. The 8 h SWC values from the three fixed CRNP are plotted in Figure 2 and provided in Table S3 in the supporting information.

Following the procedures described above, we processed the individual points of each of the 22 rover surveys in the same manner. In order to assign the spatial location of an observation, we take the midpoint between successive rover locations, which were recorded once per minute. However, we note that the midpoint is representative of an elliptical area due to the nature of CRNP neutron counts summed over 1 min intervals and the CRNP measurement area of ~300 m radius and the distance between driving points. Given the maximum driving speed of 0.8 km/min, the largest measurement area would be an ellipse with major axis = 1400 m and minor axis = 600 m. After computing the neutron correction factors and assigning the observation midpoint, we use an ordinary kriging procedure with an exponential model to perform a spatial interpolation of the 12 km × 12 km domain with a resolution of 250 m. A resolution of 250 m was chosen, as it is convenient for the spatial scaling analyses, where the entire domain is 48 × 48 and divisible by integers of 2, 3, 4, 6, 8, 12, 16, and 24. Table S4 in the supporting information summarizes the estimates of the sill, range, and R^2 (all > 0.89) for each of the sampling dates. We estimate $N_{0,F}(\mathrm{BWE})$ for all points in time and space (see Table S4 in the supporting information) using the available data sets of land use (Figure 1b and Table S6 in the supporting information), vegetation sampling during calibration dates (Table S2 in the supporting information), and using a linear interpolation with time between calibration dates. For wetland areas, we assumed a similar growth rate and change in BWE as the soybeans, and for built-up areas, we assumed a BWE equal to 0. We use the average parameter estimates of θ_{LW}, θ_{SOC}, and ρ_b from the calibration data sets (Table S2 in the supporting information) for all points in the domain in order to specify the remaining parameters needed by equation (1) to convert neutron counts into SWC, see Figures 3c and 3d for example rover SWC values. Available soil maps from the NRCS indicate a fairly homogeneous surface soil texture (i.e., ~90% silt loam and ~10% silty clay loam in the top 30 cm) in the study area. We do note the influence of the dry gravel roads on the SWC in Figures 3c and 3d. Table S6 in the supporting information summarizes the kriged neutron counts and SWC from all rover surveys. Figure 2 illustrates the mean values of all rover surveys showing temporal behavior consistent with the fixed probe values but with consistently lower absolute values. The differences in the absolute values are likely due to the fact that the rover surveys were all collected from the single-lane gravel and paved roadways. We note that during calibration sampling, the rover was driven to within 5 m of the fixed probe and showed consistent behavior indicating the likely influence of the dry roadways on the rover surveys. Future efforts may consider reducing or removing the effects of dry roadways or dry field corners on SWC values, particularly if using them to help schedule irrigation of an agricultural field.
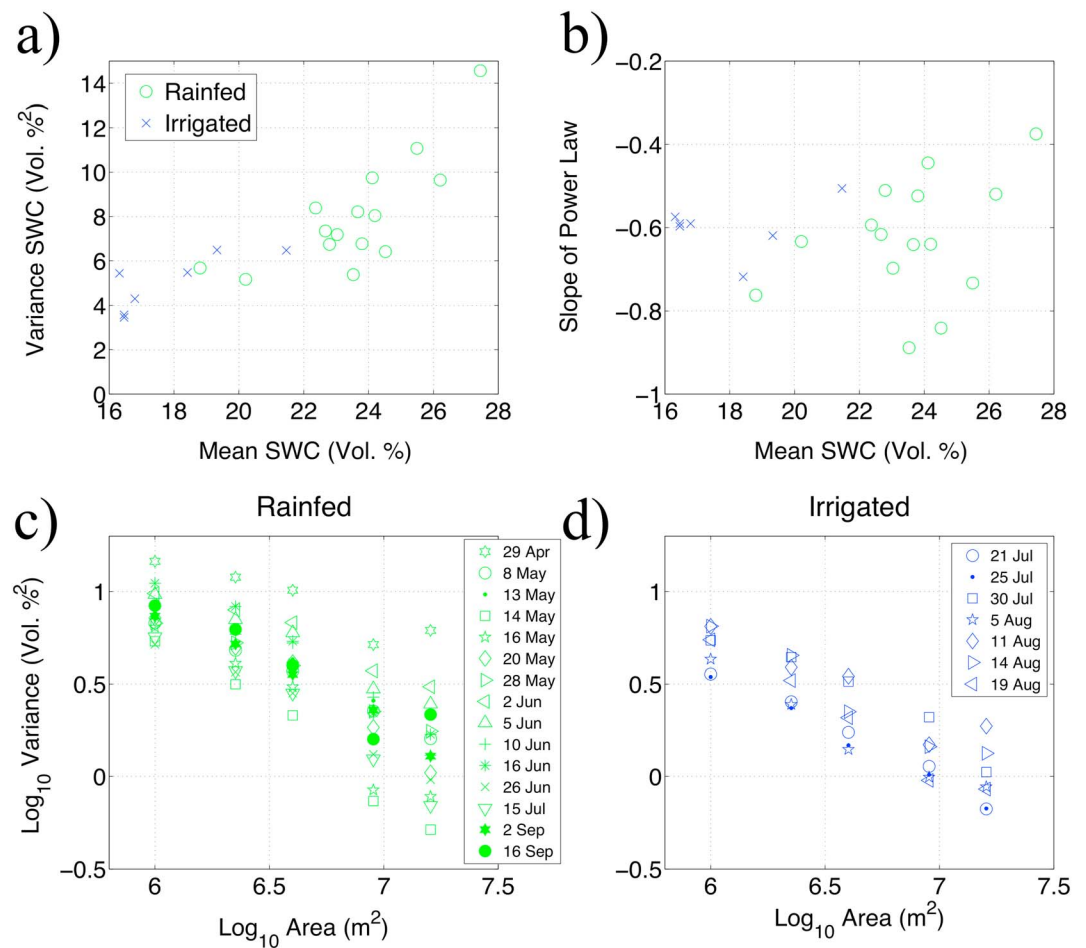
Figure 4. (a) Relationship between the mean soil water content (1 km resolution) and variance of soil water content organized by rainfed and irrigated periods. (b) Slope of the log area versus log variance plotted versus mean soil water content. (c and d) Log variance versus log area relationships for different rover sample dates and organized by rainfed and irrigated periods. Data sets and statistical analysis are provided in Tables S7 and S8 in the supporting information.

5. Results

5.1. Spatiotemporal Statistical Analysis

Table S7 in the supporting information reports the mean, variance, skewness, kurtosis, coefficient of variation, and median SWC of the 12 km × 12 km study area at aggregate spatial resolutions of 1 and 3 km for each of the 22 surveys. We find that a strong linear relationship (see Figure 4a and Table S8 in the supporting information for R^2 and P values) exists between the mean and variance at both spatial resolutions as reported by others [*Crow et al.*, 2012]. The limited range of observed mean values (16 to 27%) likely limits the expected inverted parabolic shape reported elsewhere [*Crow et al.*, 2012]. We found no consistent statistically significant linear relationships existed between (1) the mean and higher order moments, (2) the mean and the range of the semivariogram, or (3) by partitioning the observations into time periods of predominantly rainfed and irrigated (Figure 4a).

Table S9 in the supporting information and Figures 4b–4d summarize a spatial scaling analysis [*Rodriguez-Iturbe et al.*, 1995] indicating that the log of the averaging area versus the log of the SWC variance follow a power law with all sample dates having an R^2 over 0.9. The analysis indicated no statistically significant relationship between the slope of the power law function versus the mean soil moisture ($R^2 = 0.14$, P value = 0.18 for rainfed periods and $R^2 = 0.07$, P value = 0.57 for irrigated periods) as reported elsewhere [*Rodriguez-Iturbe et al.*, 1995]. A preliminary fractal analysis using exceedance probabilities of SWC islands [*Rodriguez-Iturbe et al.*, 1995] indicated fractal and multifractal signatures. However, samples sizes of SWC islands were small
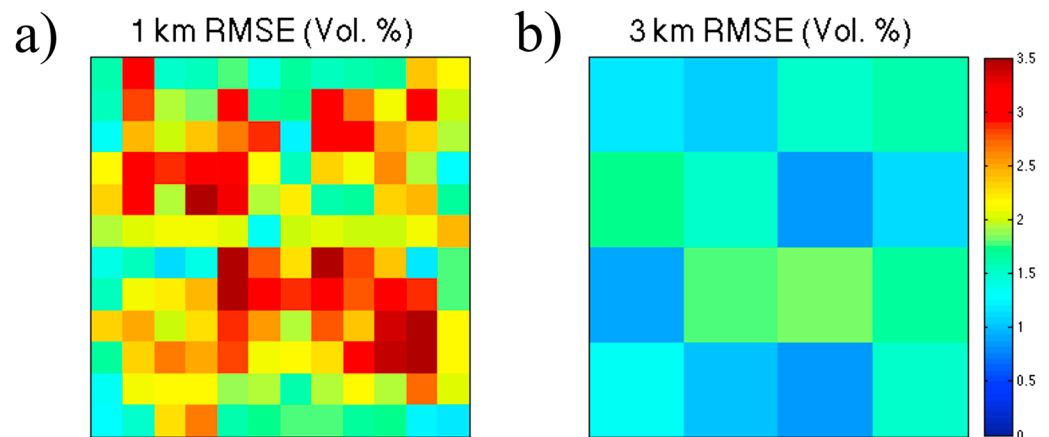
Figure 5. RMSE of linear relationship between average of three fixed probes and rover SWC estimates for (a) 1 km and (b) 3 km resolutions. Data sets are provided in Table S13 in the supporting information.

($n < 30$), limiting the robustness of the analysis. Future rover surveys that cover larger areas (~40 km × 40 km) should generate more SWC islands ($n > 200$) in order to provide sufficient sample sizes to gain further insight about the fractal nature of soil moisture fields in agricultural areas of eastern Nebraska.

Table S10 in the supporting information summarizes the temporal covariance matrix at 1 and 3 km aggregation scales. We assembled the temporal covariance matrix by selecting paired points at the same grid location and resolution between sampling dates. As reported elsewhere [*Brocca et al.*, 2012], the diagonals are the dominant terms indicating the high spatial variability within a sampling day as compared between sampling dates. The off-diagonal terms indicate that the correlation dies off quickly and is not well captured by our weekly sampling. Tables S11 and S12 in the supporting information summarize the spatial covariance matrices at 1 and 3 km aggregation scales. We assembled the spatial covariance matrix by selecting paired points between various grid locations on the same sampling date. As with the temporal covariance, the diagonal terms are largest with the off-diagonals oscillating with values close to zero. By investigating the spatial and temporal covariance matrices, we find that relative magnitudes of the diagonals are much larger than the off-diagonals. The reduction of the covariance matrix to its diagonal components is a significant simplification for performing statistical downscaling of remotely sensed products or LSM model outputs following previous methods [*Vrugt et al.*, 2003].

5.2. Spatial Regression and Data Merging

Table S13 in the supporting information and Figure 5 summarize a leave-one-out cross-validation linear regression analysis for aggregation scales of 1, 3, and 12 km following *Ford and Quiring* [2014]. The linear regression coefficients for each grid cell were estimated by comparing the average SWC of the three fixed CRNP versus the corresponding rover SWC value for that grid cell at 1, 3, and 12 km resolutions for each sampling date. Coefficients and root-mean-square error (RMSE) values were estimated by leaving one survey date out of the regression analysis and repeating the procedure until all surveys had been removed and added. The average coefficients and RMSE values are then reported. Table S13 in the supporting information provides the grid cell location, the average best fit intercept and slope, RMSE, and R^2 of the linear regression analysis. The 12 km resolution resulted in a low RMSE of 0.86%, the 3 km resolution resulted in RMSE values for all grid cells less than 1.83%, and the 1 km resolution resulted in 85.4% of grid values with RMSE less than 3%. The highest RMSE values were predominantly located in the built up environment and wetland areas where the CRNP did not adequately capture the SWC dynamics. Video S1 in the supporting information illustrates the 8 h 1 km derived soil moisture product and consistently follows wetting patterns from the available rainfall and irrigation time series. We note that we assume that the relationship between fixed measurements and each pixel in the SWC map remains the same over time. While the data confirms this assumption here, we suggest that future studies verify this behavior. In particular for larger averaging areas, where the degree of heterogeneity in soil, land use and climatic conditions may violate this assumption.

6. Discussion

With the fixed CRNP SWC values (Table S3 in the supporting information) and linear regression coefficients (Table S13 in the supporting information) distributed in space, a continuous monitoring network of SWC and associated RMSE can be produced at the various grid aggregations of 1, 3, and 12 km. We note that the intercept and slope appear fairly constant over the study period as indicated by the leave-one-out cross-validation analysis. However, this finding should be further validated by repeating the experiment with significantly longer periods of irrigation at this study site or in drier environments where more contrast in SWC between irrigated and rainfed areas is likely to exist. Future studies should consider the selection of the representative fixed CRNP within the study area, relative weighting of each fixed CRNP SWC value, or inclusion of ancillary data (i.e., soil type, topography, and vegetation type) to further improve the regression analysis [*Coopersmith et al.*, 2014] and overall performance of the SWC monitoring network.

7. Conclusions

In this work, we present a proof-of-concept study for designing a cost-effective and real-time soil moisture-monitoring network at the critical 1 km spatial resolution that can cover 10^2 to 10^3 km^2. The network design fills a critical gap in soil moisture observations that will be beneficial for (1) the next generation of hyperresolution land surface models that will investigate areas such as optimal water management in irrigation, (2) the strength of land-atmospheric coupling, (3) calibration and validation of satellite remote sensing products, and (4) value addition to satellite remote sensing products by spatial downscaling.

References

Bogena, H. R., J. A. Huisman, R. Baatz, H. J. H. Franssen, and H. Vereecken (2013), Accuracy of the cosmic-ray soil water content probe in humid forest ecosystems: The worst case scenario, *Water Resour. Res.*, 49(9), 5778–5791, doi:10.1002/wrcr.20463.

Brocca, L., T. Tullo, F. Melone, T. Moramarco, and R. Morbidelli (2012), Catchment scale soil moisture spatial-temporal variability, *J. Hydrol.*, 422, 63–75.

Chrisman, B., and M. Zreda (2013), Quantifying mesoscale soil moisture with the cosmic-ray rover, *Hydrol. Earth Syst. Sci.*, 17(12), 5097–5108, doi:10.5194/hess-17-5097-2013.

Coopersmith, E. J., B. S. Minsker, and M. Sivapalan (2014), Using similarity of soil texture and hydroclimate to enhance soil moisture estimation, *Hydrol. Earth Syst. Sci.*, 18(8), 3095–3107, doi:10.5194/hess-18-3095-2014.

Crow, W. T., A. A. Berg, M. H. Cosh, A. Loew, B. P. Mohanty, R. Panciera, P. de Rosnay, D. Ryu, and J. P. Walker (2012), Upscaling sparse ground-based soil moisture observations for the validation of coarse-resolution satellite soil moisture products, *Rev. Geophys.*, 50, doi:10.1029/2011RG000372.

Desilets, D., and M. Zreda (2013), Footprint diameter for a cosmic-ray soil moisture probe: Theory and Monte Carlo simulations, *Water Resour. Res.*, doi:10.1002/wrcr.20187.

Desilets, D., M. Zreda, and T. P. A. Ferre (2010), Nature's neutron probe: Land surface hydrology at an elusive scale with cosmic rays, *Water Resour. Res.*, 46, doi:10.1029/2009WR008726.

Dong, J. N., T. E. Ochsner, M. Zreda, M. H. Cosh, and C. B. Zou (2014), Calibration and validation of the COSMOS rover for surface soil moisture measurement, *Vadose Zone J.*, 13(4), doi:10.2136/vzj2013.08.0148.

Ford, T. W., and S. M. Quiring (2014), Comparison and application of multiple methods for temporal interpolation of daily soil moisture, *Int. J. Climatol.*, 34(8), 2604–2621, doi:10.1002/joc.3862.

Franz, T. E., M. Zreda, P. A. Ferre, R. Rosolem, C. Zweck, S. Stillman, X. Zeng, and W. J. Shuttleworth (2012), Measurement depth of the cosmic-ray soil moisture probe affected by hydrogen from various sources, *Water Resour. Res.*, 48, doi:10.1029/2012WR011871.

McJannet, D., T. E. Franz, A. Hawdon, D. Boadle, B. Baker, A. Almeida, R. Silberstein, T. Lambert, and D. Desilets (2014), Field testing of the universal calibration function for determination of soil moisture with cosmic-ray neutrons, *Water Resour. Res.*, 50(6), 5235–5248, doi:10.1002/2014WR015513.

Nelson, D. W., and L. E. Sommers (1996), Total carbon, organic carbon, and organic matter, in *Methods of Soil Analysis, Part 2*, 2nd ed., edited by A. L. Page, pp. 961–1010, Am. Soc. of Agronomy, Madison.

Ochsner, T. E., et al. (2013), State of the art in large-scale soil moisture monitoring, *Soil Sci. Soc. Am. J.*, 77(6), 1888–1919, doi:10.2136/sssaj2013.03.0093.

Rodriguez-Iturbe, I., G. K. Vogel, R. Rigon, D. Entekhabi, F. Castelli, and A. Rinaldo (1995), On the spatial-organization of soil-moisture fields, *Geophys. Res. Lett.*, 22(20), 2757–2760, doi:10.1029/95GL02779.

Santanello, J. A., C. D. Peters-Lidard, and S. V. Kumar (2011), Diagnosing the sensitivity of local land-atmosphere coupling via the soil moisture-boundary layer interaction, *J. Hydrometeorol.*, 12(5), 766–786, doi:10.1175/jhm-d-10-05014.1.

Vrugt, J. A., H. V. Gupta, W. Bouten, and S. Sorooshian (2003), A Shuffled Complex Evolution Metropolis algorithm for optimization and uncertainty assessment of hydrologic model parameters, *Water Resour. Res.*, 39(8), 1201, doi:10.1029/2002WR001642.

Wood, A. W., L. R. Leung, V. Sridhar, and D. P. Lettenmaier (2004), Hydrologic implications of dynamical and statistical approaches to downscaling climate model outputs, *Clim. Change*, 62(1–3), 189–216, doi:10.1023/B:CLIM.0000013685.99609.9e.

Wood, E. F., et al. (2011), Hyperresolution global land surface modeling: Meeting a grand challenge for monitoring Earth's terrestrial water, *Water Resour. Res.*, 47, W05301, doi:10.1029/2010WR010090.

Zreda, M., W. J. Shuttleworth, X. Xeng, C. Zweck, D. Desilets, T. E. Franz, and R. Rosolem (2012), COSMOS: The cosmic-ray soil moisture observing system, *Hydrol. Earth Syst. Sci.*, 16, 4079–4099, doi:10.5194/hess-16-1-2012.

Geophysical Research Letters

Supporting Information for

Spatiotemporal characterization of soil moisture fields using cosmic-ray neutron probes and data fusion

T.E. Franz[1], T. Wang[1], W. Avery[1], C. Finkenbiner[1], L. Brocca[2]

[1]University of Nebraska-Lincoln, Nebraska 68583 USA

[2]Istituto di Ricerca per la Protezione Idrogeologica, Perugia, IT

Contents of this file

Additional Supporting Information (Files uploaded separately)

Captions for Datasets S1 to S13
Captions for Movie S1

Introduction

This supporting information contains 13 datasets that support the 5 figures in the manuscript. The datasets describe the 11 calibration datasets of the cosmic-ray probes, the 3 time series of fixed cosmic-ray probe data, the 22 cosmic-ray rover datasets, the landcover, the cosmic-ray rover geostatistics, the spatiotemporal statistics of cosmic-ray rover results, and the data fusion regression coefficients. This supporting information also contains 1 avi movie file illustrating the 8-hr 1 km resolution soil moisture product and corresponding rainfall and irrigation events.

Data Set S1. Summary of 11 calibration datasets from the 3 fixed cosmic-ray neutron probes. On 9 of the 11 calibration dates it was possible to drive the cosmic-ray rover within 5 m of the fixed probe site for cross calibration. The 108 gravimetric water content and soil bulk density estimates are provided from each of the 18 sampling locations and 6 depths. A 30 cm long split tube sampler with a 5 cm diameter was used to collect the gravimetric and bulk density samples.

Data Set S2. Summary of fixed and rover cosmic-ray neutron counts during calibration. Soil sampling results reporting the average gravimetric water content, soil bulk density, soil lattice water and soil organic carbon water equivalent are also summarized. Soil chemistry samples from 1 calibration date were sent to Actlabs (Ontario, Canada) for analysis. Biomass sampling results are also summarized. Biomass estimates were collected at 6 points from around the footprint and consisted of estimating the number of plants per unit area, clipping, weighing, and drying biomass samples (typically 1 to 3 plants per site). Calculations of N_0 for the fixed and rover are computed from the datasets using equation (1) and average estimates of soil bulk density, lattice water, and soil organic carbon water equivalence.

Data Set S3. Summary of 8-hour estimates of *SWC* for the 3 fixed cosmic-ray neutron probes. The time varying N_0 values summarized in DS02 were used with Eq. [4].

Data Set S4. Summary of semivariogram from 22 rover surveys reporting the sill, range, and R^2. An exponential model with no nugget was used as the variogram model. A simple ordinary kriging algorithm was used with the exponential model fit to generate the spatial interpolation of the neutron counts over the domain.

Data Set S5. Summary of N_0 values by landcover and date. For the builtup environment we assumed a constant N_0 value and for the natural areas we assumed the same N_0 as the soybeans given the similar standing biomasses of tall grass prairies and soybeans.

Data Set S6. Summary of rover survey results for a 48 by 48 grid with a 250 m resolution. The dataset includes the UTM coordinate location, estimate of landcover, spatially interpolated neutron counts, and *SWC* values.

Data Set S7. Summary of rover survey *SWC* statistical moments at 1 and 3 km aggregate resolutions.

Data Set S8. Summary of linear regression results between mean *SWC* and higher order moments at 1 and 3 km aggregate resolutions.

Data Set S9. Summary of power law fit between the log area and log *SWC* variance for each sampling date.

Data Set S10. Summary of *SWC* temporal covariance matrix at 1 and 3 km aggregate resolutions.

Data Set S11. Summary of SWC spatial covariance matrix at 1 km resolution for each sampling date. The area locations coordinates in UTM of the two samples are also provided for reference.

Data Set S12. Summary of SWC spatial covariance matrix at 3 km resolution for each sampling date. The area locations coordinates in UTM of the two samples are also provided for reference.

Data Set S13. Spatial linear regression fits and coefficients between the average of the 3 fixed cosmic-ray *SWC* (provided in DS3) and the rover estimates for 1, 3, 12 km aggregate resolutions. The grid location coordinates are provided for reference.

Movie S1. Summary movie of 8-hr 1 km soil moisture product with corresponding rainfall and irrigation time series.